Collège de France LPC/95-08
CERN-LAA/95-11
20/3/95

Flavor and flux determination of the pp solar neutrinos via $\nu - e$ elastic scattering

J. Séguinot and T. Ypsilantis
Collège de France, Paris, France

G. Bonvicini
CERN, Geneva, Switzerland

P. Giusti, G. Laurenti and A. Zichichi
I.N.F.N. Bologna, Italy

Abstract :

Elastic νe scatters in a large helium TPC gas volume ($\approx 2000\,\mathrm{m}^3$) can be observed by detection of electron recoil tracks. Values of the track kinetic energy T and direction θ (for a given solar position) suffice to determine the incident neutrino neutrino energy E_ν. These quantities can be inferred from long drift collection of ionization electrons on the TPC detector plane. The obtainable energy resolution ($\sigma_{E\nu}/E_\nu$) should vary from 3 to 7 % at $E_\nu = 300\,\mathrm{keV}$ and 3 to 18 % at $E_\nu = 862\,\mathrm{keV}$. High event rates ($\approx 4000/\mathrm{yr}$) can be obtained by increasing the He gas density (a factor 20) by operating at (5 bars, 77°K) even though this limits the mesurable electron recoil energy to $T \simeq$ 50-100 keV.

The flavor mix $f = n_{\nu\mu}/(n_{\nu e} + n_{\nu\mu})$ and absolute flux ϕ of the incoming solar neutrinos may be found from the T distribution and rate of electron recoils. The cross section σ_{tot} and $d\sigma/dT$, known from electro-weak theory, are sufficiently different for $\nu_e e \to \nu_e e$ (NC + CC) and $\nu_\mu e \to \nu_\mu e$ (NC) channels to allow sensitive determination of (f, ϕ) independently of solar models or mixing scenarios.

Résumé :

La diffusion élastique νe peut être observée par la détection de la trace de l'électron de recul dans une chambre à projection temporelle (TPC) de grand volume ($\sim 2000\,\mathrm{m}^3$) remplie d'hélium. Les mesures de l'énergie cinétique T de l'électron et de sa direction θ déterminent l'énergie du neutrino incident, connaissant la position du soleil. La résolution en énergie ($\sigma_{E\nu}/E_\nu$) devrait varier entre 3 et 7 % pour $E_\nu = 300\,\mathrm{keV}$ et 3 à 18 % pour $E_\nu = 862\,\mathrm{keV}$. Un taux de détection de ~ 4000 ν/an peut être obtenu en augmentant la densité de l'hélium par un facteur 20 avec une pression de fonctionnement de 5 bars à 77°K, mais en limitant l'énergie mesurable de l'électron de recul à $T \simeq 50$–$100\,\mathrm{keV}$.

Le facteur de mélange des saveurs $f = n_{\nu\mu}/(n_{\nu e} - n_{\nu\mu})$ et le flux absolu ϕ des neutrinos solaires incidents peuvent être déduits de la distribution de l'énergie cinétique des électrons T et de leur taux de détection. Les sections efficaces σ_{tot} et $d\sigma/dT$ dérivées de la théorie électrofaible sont bien connues et suffisamment différentes pour les réactions $\nu_e e \to \nu_e e$ (NC + CC) et $\nu_\mu e \to \nu_\mu e$ (NC), pour permettre une détermination de (f, ϕ) indépendamment du modèle solaire ou des combinaisons possibles de mélange des saveurs.

1 Review of the HELLAZ experiment

A real time experiment to detect and measure the energy of solar neutrinos has been previously described by Séguinot, Ypsilantis and Zichichi [1]. It is mostly sensitive to pp and ^{7}Be neutrinos and to a lesser degree to the p-e-p, ^{15}O and ^{13}N sources. Subsequently, several publications [2, 3, 4] have described the evolution and progress of this work.

The experiment called HELLAZ (HELium at Liquid AZote temperature) consists of a large helium gas volume ($\approx 2000\,\mathrm{m}^3$, 5 bar, 77°K, 6 tons) which is the target for νe elastic scatters. The recoil electron from a νe scatter will stop in the He gas leaving a trail of ionization electrons defining a track. These electrons will then drift in an applied axial electric field until they reach a two-dimensional (x, y) detector located at the end of the drift volume. The third (z) coordinate of a point on the track locus is determined by the arrival time of the electron. These data determine the electron energy and direction and, given the sun's position, the neutrino energy.

The νe events rate for the pp and ^{7}Be fluxes, calculated from the Bahcall solar model [5], is $\approx 10^3$/ton-y hence, for the 6 ton He gas target, 6000/y (16/d) assuming all recoil electrons ($T \geq 0$) are detected. With a realistic detection limit ($T \geq 100$ keV), the event rate is 2500/yr (7/d), still enormous compared to radiochemical, inverse β, threshold E_ν detectors (0.1–0.3/d). Total event rates in $2000\,\mathrm{m}^3$ HELLAZ ($n_e = 2 \cdot 10^{30}$ e, $T_{\min} = 100\,\mathrm{keV}$) will be 2500/y for pp, 1500/y for ^{7}Be, 100/y for pep, 170/y for ^{13}N and 220/y for ^{15}O. The low-flux ^{8}B and ^{17}F sources ($\approx 6 \cdot 10^6/\mathrm{cm}^2$-s) however will not be significantly sampled (20/y and 2/y, respectively).

At the HELLAZ gas density ($3\,\mathrm{kg/m}^3$ of He + H_2/CH_4), even low energy ($T \geq 100\,\mathrm{keV}$)

electrons have sufficient range ($R \geq 50\,\mathrm{mm}$) to be measurable allowing electron direction and energy to be determined with error ($\sigma_\theta \approx 35\,\mathrm{mrad}$, $\sigma_T/T \approx 3\,\%$). These then give the neutrino energy with error $2\,\% < \sigma_{E\nu}/E_\nu < 4\,\%$ for $E_\nu = 300\,\mathrm{keV}$. In contrast, none of the existant or proposed neutrino detectors has any significant neutrino energy resolution [4].

A transverse view of the cylindrical TPC is shown in Fig.1. It has longitudinal drift regions of $\pm 10\,\mathrm{m}$ terminated at each end by ionization detectors to measure the electron track locus. The detectors must operate in the same drift gas mixture with sufficient gain to attain significant single electron efficiency ($> 90\,\%$). This allows identification of the track head/tail and determines track direction. In addition, single electron counting allows a measurement of T (in addition to range) thereby endowing the detector with a calorimetric capability.

A critical feature of HELLAZ is the shield needed to absorb gammas and neutrons coming from the cavern walls. We propose a shield of solid CO_2 because it is radiopure, cheap, strong, dense (1.6 g/cm^3), and cold [6, 7]. The low temperature (180°K) shield is important because it condenses difficult impurities such as radon, which would otherwise diffuse as a gas into the TPC volume. In general, HELLAZ will require very high purity of all component materials.

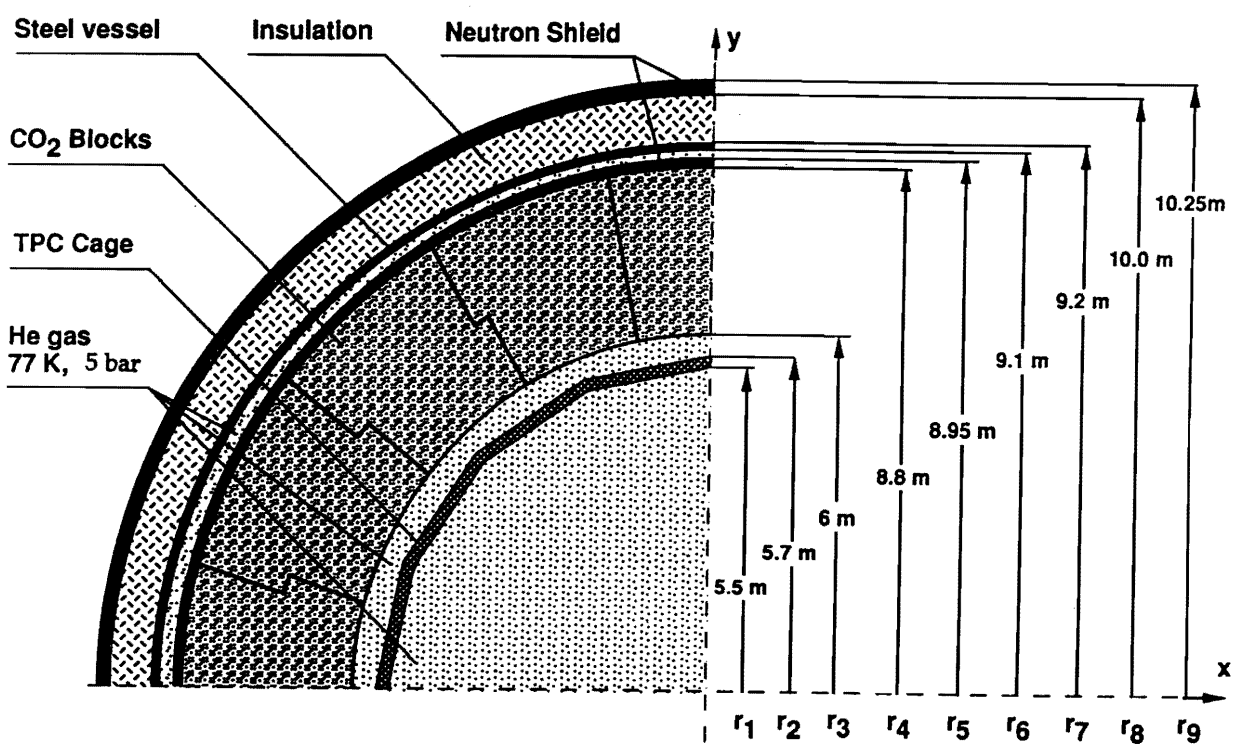

Figure 1: A transverse view of the HELLAZ TPC and shield.

1.1 The MultiWire Chamber (MWC) Detector Option

Each $100\,\mathrm{m}^2$ endcap would be composed of $1\,\mathrm{m}^2$ modular detectors made of 10 mm thick Kevlar honeycomb planes with $100\,\mu\mathrm{m}$ thick Kevlar-Epoxy skins. The inner surface of each section is covered by a $100\,\mu\mathrm{m}$ thick Kapton layer on which 0.95 mm wide metallic cathode strips are deposited along x (1 mm pitch in y). The 1 m long MWC wires are strung along y (1 mm pitch in x). The anode wire-cathode strip distance is fixed by 2 mm thick quartz spacers placed at 10 cm intervals along x. A smaller anode-cathode gap (0.5 mm) was found essential to obtain good single electron-cathode strip efficiency ($\geq 97\,\%$) in 1 bar CH_4 gas [8] but at the higher density of HELLAZ, a 2 mm spacer should suffice.

The energy resolution of a MWC is usually dominated by fluctuations in amplification however, if the MWC has good single electron sensitivity (SES) then only ionization fluctuations are important. Energy loss in He gas is, however, a special case because of the dominant energy loss processes are ionization and scintillation with very little energy lost to excitons. For example, a $T = 100\,\mathrm{keV}$ electron in He produces a total of about 2500 electrons and about 2000 UV photons ($\tau \leq 2\,\mathrm{ns}, \lambda_{\mathrm{ph}} \approx 60\,\mathrm{mm}$, $E_{\mathrm{ph}} = 21.2\,\mathrm{eV}$) accounting for almost all the 100 keV energy deposited. The (H_2/CH_4) total absorption cross section at 21.2 eV is (7/30) Mb of which (100 % / 50 %) is photoionizing, thus the He scintillation photons will photoionize (H_2/CH_4) causing photoelectrons to be injected into the TPC gas very near the track locus ($l_{\mathrm{abs}} \approx 100\,\mu\mathrm{m}$) allowing an important fraction of the scintillation energy to be recovered as ionization. Simple counting of the (4500/3500) electrons could then give an energy resolution $\sigma_T/\sqrt{T} = 1/\sqrt{N} \approx (1.5/1.7)\,\%$. We have already developed SES-MWCs for Cherenkov ring imaging [8].

The silicon pre-amplifier electronics developed for the Liquid Argon Accordion Calorimeter [9] at 87°K should suffice for HELLAZ but we are also studying cold Ge and GaAs circuits.

A 16 bit time-to-digital-converter (TDC) with 20 ns time bins observes 1.3 ms of drift time (i.e. a track length of $\approx 1\,\mathrm{m}$ or 10 % of the total). This type of electronics is commercially available but perhaps a VLSI version must be developed for HELLAZ.

A trigger to start data acquisition will be obtained from a coincidence of contiguous wires and/or strips of the MWC. This occurs when the first electrons of the track arrive at the detector plane. Thus, the absolute z position of the track is not determined, but is not needed to obtain the track direction and energy.

1.2 The Hybrid Photo-Diode (HPD) Detector Option

The recently developed HPD has a vacuum photocathode coupled to a SES silicon strip detector [10]. It may also be used as the SES ionization detector. An incoming ionization electron would encounter a high field ($\approx$ 10 kV/cm) pre-amplification region just preceding the quartz-windowed HPD photon detector. In a gas mixture of He + 10 % H_2,

an amplification process will occur in the high field region causing electron multiplication (by a factor M) and photon production (factor L) with ratio $L/M \approx 0.1$–1. These photons (160 nm in He + H_2) are produced predominantly near the quartz window and will transmit through the quartz window only locally (thus preserving the spatial position) to encounter a CsI transmittive photocathode. Even though the quantum efficiency of the photocathode is only 10 %, pre-amplification by factor $M \approx 200$–20 would result in L ≈ 20 (photons per incident ionization electron). This small amplification factor ($M \approx 200$–20) is easily attainable in a gap of several millimeters. The HPD photoelectron, accelerated to ≈ 20 kV in the HPD vacuum, impinges onto a silicon strip detector [11] to produce ≈ 5000 electron/hole pairs. The electrons are collected on x cathode strips and the holes on the opposite y cathode strips. As before, this gives a single unambiguous pixel hit (x, y) if only a single electron is incident in the given 20 ns time bin. An HPD of $100 \times 100\,\mathrm{mm}^2$ will require 200 strip readout channels, thus two VA2 chips of 128 channels each [12]. These chips are designed to work at LHC with time stamping every 25 ns.

Helium gas is notorious for destroying glass-windowed PM's due to permeation, however a cold, thick (single or double) quartz envelope can reduce this effect to a negligible level.

2 Track Definition

The active TPC volume is defined by a cylindrically symmetric decahexahedron of radius 5.5 m and length 20 m filled with (He + 10 % H_2 or CH_4) gas at 77°K and 5 bar. The z coordinate is defined as the cylinder axis with the horizontal (x) and vertical (y) axes shown in Fig. 1. A uniform electric field, parallel to the z axis (outward from $z = 0$), causes the ionization (and photo-)electrons to drift to the detectors.

The ionization detectors, located at the $z = \pm 10$ m endcaps, measure the position and arrival time of incoming electrons via x (wires or strips) and y strips. The timing data is obtained in 20 ns time bins for each (x, y) projections.

Nine 100-keV electron tracks, shown in Fig. 2, were generated along the z axis using the GEANT programme [13] to simulate the energy loss in the He gas. The variance of track directions are due only to multiple scattering in He gas and does not include drift diffusion. This would cause an additional 3D Gaussian smearing of each detected point by an amount $\sigma_x = \sigma_y = \sigma_t\sqrt{z}$ and $\sigma_z = \sigma_l\sqrt{z}$ where (σ_t, σ_l) are the (transverse, longitudinal) diffusion coefficients [14] in He gas (5 bar, 77°K, E = 20 kV/m) with z the drift length.

Note that the mean deflection in the first 10 mm is about 1 mm thus a directional error $\sigma_\theta \leq 100$ mrad may be expected if the sampling is sufficient. The purely ionization signal from a 100 keV electron track is about 2500 electrons distributed over the $R \approx 50$ mm range (with ≈ 2000 more from the photoionization of H_2). Good sampling statistics are feasible with a SES detector because 400 single e's are expected in the first 12 mm of the track (excluding the photoionization component) hence a statistical error of about 50

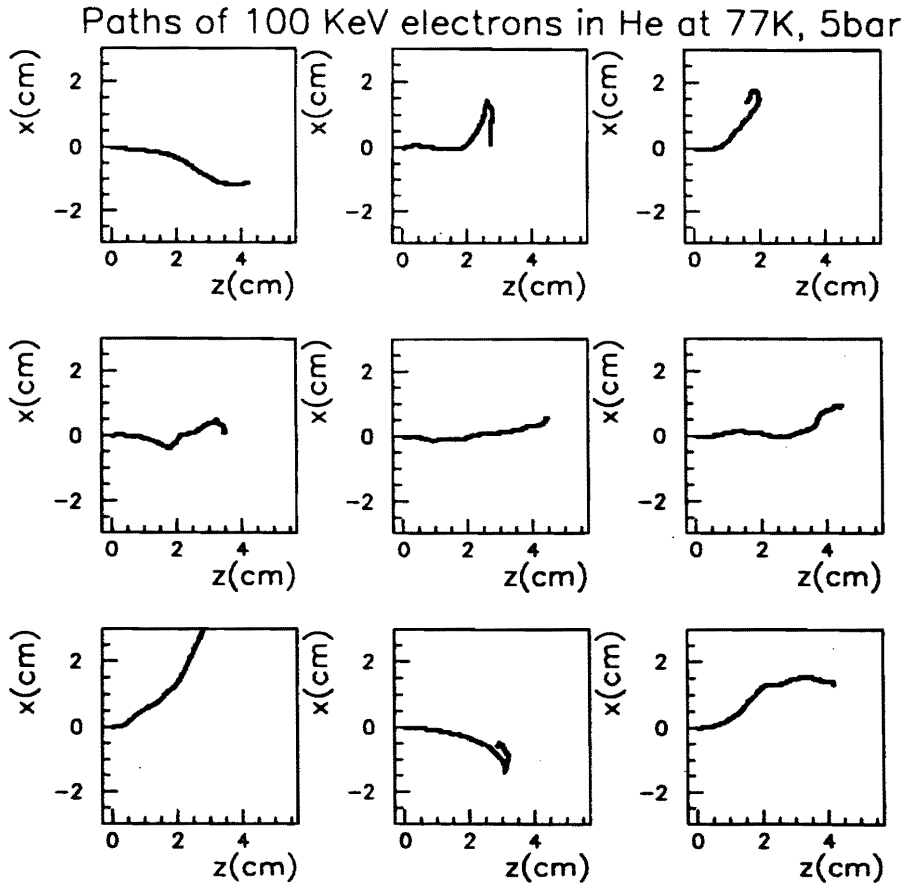

Figure 2: A GEANT simulation of nine-100 keV tracks along Z in He gas ($\rho = 3.2$ mg/cm^3) with multiple scattering but not diffusion errors.

mrad. A more precise estimate for the directional error is $\sigma_\theta = (\sigma_d/\sigma_s)/\sqrt{N}$ where σ_d is the drift diffusion error ($\langle\sigma_d\rangle = 3$ mm for 10 m drift), ($s, \sigma_s = s/\sqrt{12}$) are the (real, rms) track lengths (12, 3.5 mm) with N the number of single electrons detected (400 for $s =$ 12 mm) hence $\sigma_\theta = 43$ mrad. For a straight line fit, the sampled track length s cannot be chosen much larger because the multiple scattering deflection builds up.

Now perhaps it is clear why we require time bins $\Delta t = 20$ ns (i.e. $\Delta z = .014$ mm) even though the position error is much larger ($\langle\sigma_d\rangle = 3$ mm). It assures good sampling because each electron arrives alone and is efficiently detected by the SES detector. In addition, SES avoids the ambiguities inherent in projective readout and, as a bonus endows the detector with a calorimetric capability.

Before fitting a straight line to a track (i.e. to the cloud of single electron points) we calculate the principal axes of the cloud by diagonalizing its moment of inertia tensor [15]. We see in Fig. 3 distributions for three 100 keV tracks (the first three of Fig. 2) projected onto the three principal axes ($\langle\sigma_d\rangle = 3$ mm is included).

The distributions along the principal y and z axes are symmetric with $\sigma_y \approx \sigma_z \approx 3$ mm,

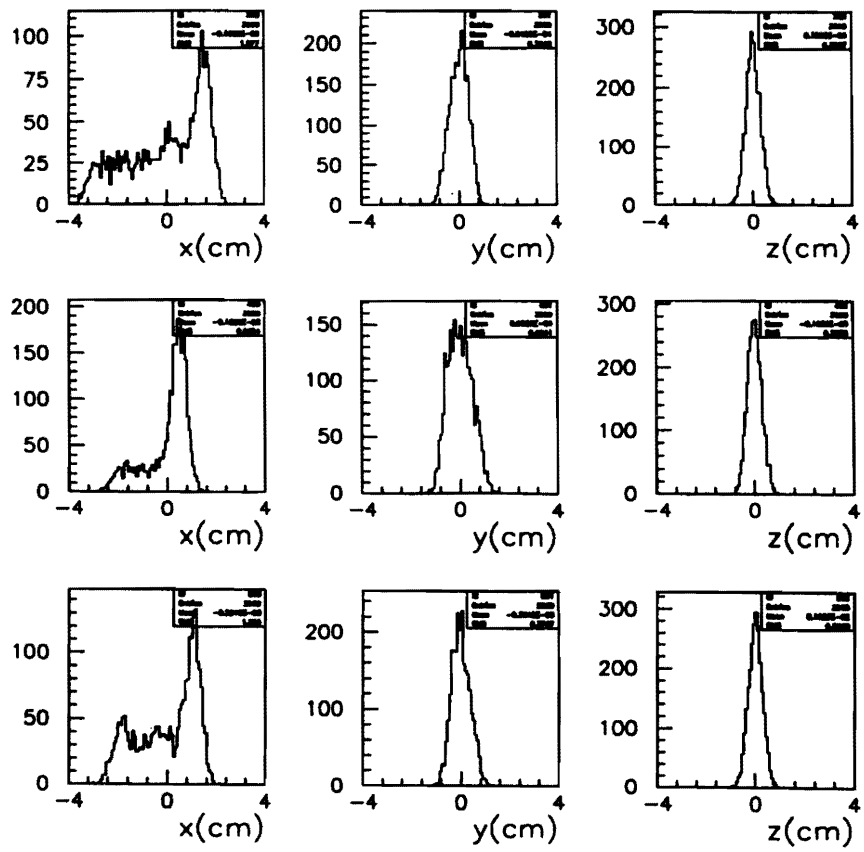

Figure 3: Distribution of hits along principle axes (the first three tracks of figure 2) with both multiple scattering and drift diffusion (z = 9 m) errors included.

as expected, whereas the x distribution shows the track range and increased ionization at the track end. The first track is well-behaved while the second and third track show the effects of large angle deflections (the range is too small for the ionization). Clearly, the track energy, range and direction are more easily calculable in this coordinate system.

3 Track direction and energy determination

The direction error σ_θ obtained fitting a straight line ($x = bz, b = \tan\theta$) to $s = 12$ mm track segments vs the drift error $\sigma_d = \sigma_{dz} = \sigma_{dx}$ is shown in Fig. 4 for 100 keV electrons and pixels sizes $\Delta x = \Delta y = 1$ mm, $\Delta z = 0.14$ mm with $N = 428$. The space point errors $\sigma_x = \sqrt{(\sigma_d^2 + \Delta x^2/12)}$ and $\sigma_z = \sqrt{(\sigma_d^2 + \Delta z^2/12)}$ and are dominated by diffusion. Note that σ_θ varies from (15 to 90 mrad) for σ_d from (0 to 4.5 mm) with average $\langle\sigma_\theta\rangle = 60$ mrad.

When the tracks are fit to the expected curve ($x' = bz'^{3/2}, x' = x\cos\theta + z\sin\theta$ and $z' = z\cos\theta - x\sin\theta$) we find σ_θ (13 to 50 mrad) for σ_d from (0 to 4 mm) thus $\langle\sigma_\theta\rangle \approx 30$ mrad.

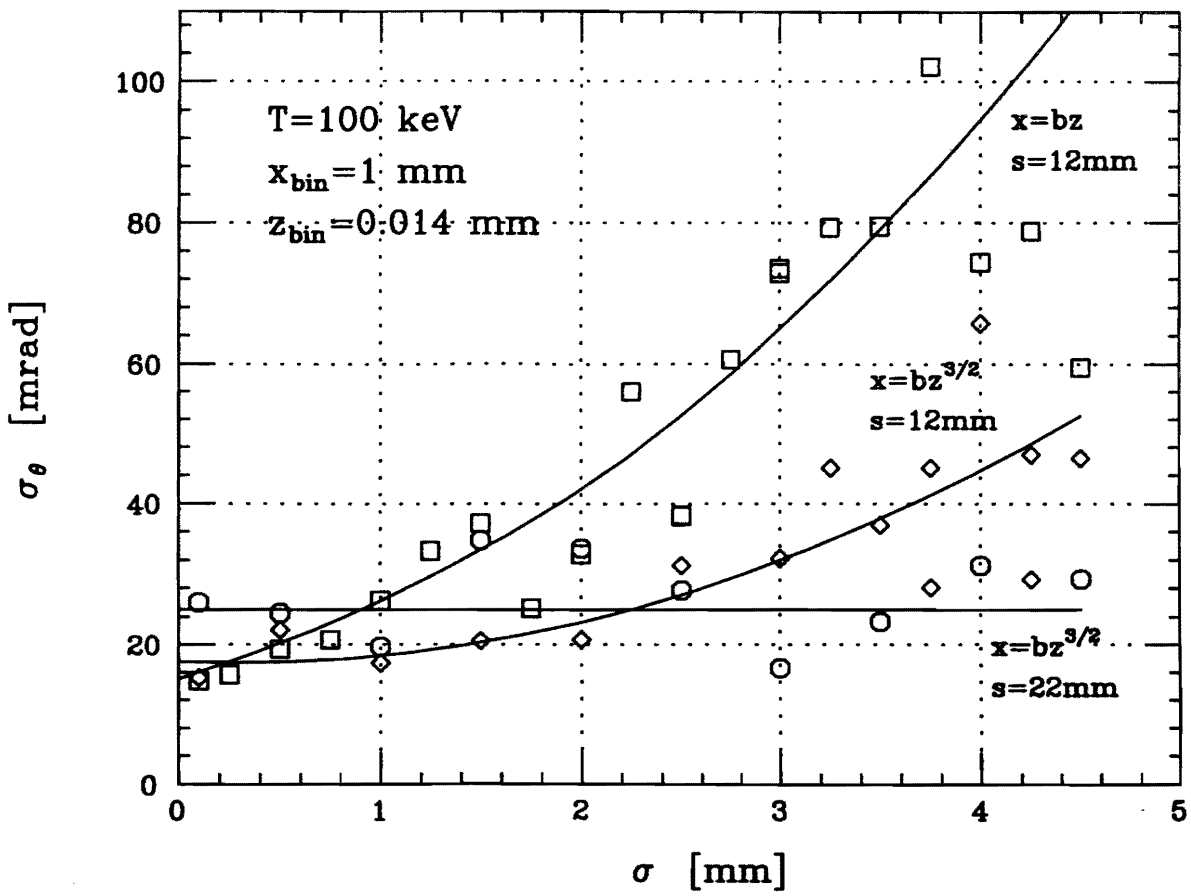

Figure 4: Direction error σ_θ for N samples of a 100 keV track vs drift error σ. The indicated fits are either to a straight line ($x' = bz'$) or to a curved line ($x' = bz'^{3/2}$).

Increasing the track length to $s = 22$ mm (hence $N = 785$) further improves the fit to $\sigma_\theta \approx 25$ mrad for σ_θ from (0 to 45 mm). These fits all use the track starting point found from the principal axis distributions of Fig. 3. Each fit is for a 2D projection (x, z) or (y, z), thus the space angle error is larger by $\sqrt{2}$ i.e. $\sigma_\theta \approx 35$ mrad.

The track energy can be determined from the track range R after the principal axis transformation (see Fig. 3). Fluctuations of σ_R/R vary from 8 % at 100 keV to 4 % at 1000 keV [13].

The resolution σ_T/T would be improved to between 2 % and 4 % if T is measured by single electron counting with a corresponding decrease in σ_{E_ν}/E_ν.Using this result with $\langle\sigma_\theta\rangle = 35$ mrad gives the neutrino energy resolution σ_{E_ν}/E_ν vs E_ν shown in Fig. 5 for fixed T contour lines. This shows that σ_{E_ν}/E_ν between 3 % to 7 % may be obtained in the pp region i.e. for E_ν between 220 and 420 keV.

For further information on the many other detector and construction issues of HELLAZ we refer the reader to [2, 3, 4]. We continue, instead, with a discussion of new aspects of the HELLAZ detector methodology.

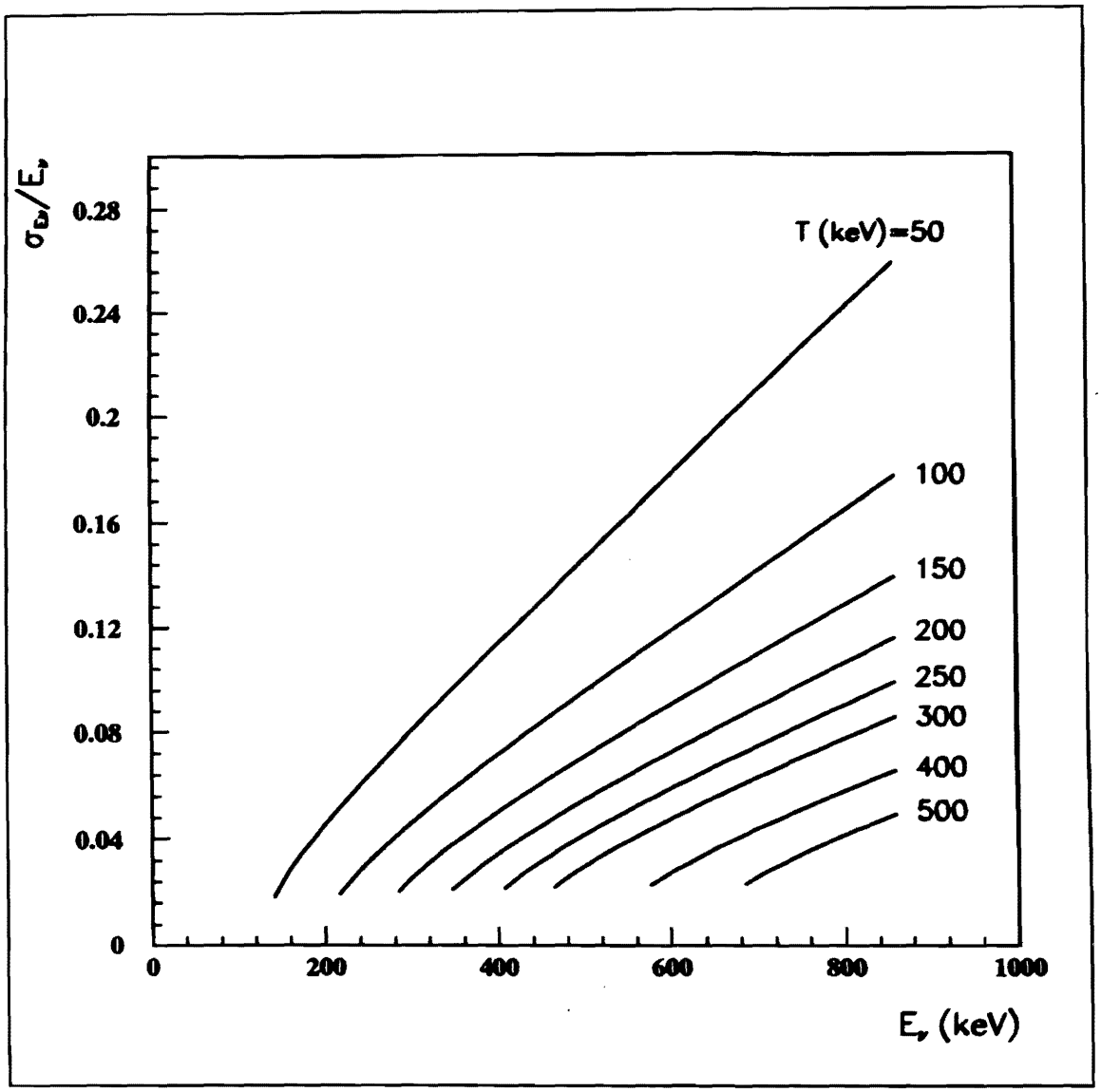

Figure 5: The neutrino resolution $\sigma_{E\nu}/E_\nu$ vs neutrino energy E_ν for fixed T (keV).

4 Solar and/or Neutrino Physics

An important advantage of HELLAZ is its capability to measure the pp solar neutrinos. Because the pp spectral shape and intensity is determined almost completely by the visible photon luminosity [5] any observed experimental difference can be uniquely attributable to new neutrino physics. This is because the νe elastic cross section is known from the standard model electro-weak theory [16] and does not rely on overlap integrals of poorly known nuclear wave functions as needed to determine the inverse β decay cross-sections.

Because HELLAZ can measure neutrino energy, the MSW phase angle is determined hence matter-dependent oscillations are observable. Other experiments average over this angle thus are less sensitive to these oscillations. The excellent neutrino energy resolution and high counting rate of HELLAZ will permit detection of neutrino oscillations via day-night or longer time modulations of the neutrino flux. Also, if neutrinos have mass and magnetic moment and are transversely polarized by the sun's magnetic field, this polarization will be manifest as an azimuthal modulation of the νe scattered intensity. Possibly the shape and width of the ^{7}Be monoenergetic line can also be measured, thus further constraining the solar models [17].

4.1 Flavor and Flux Determination

The νe elastic differential cross section [16] is

$$\frac{d\sigma}{dT} = \left(\frac{\sigma_0}{m_e}\right)\left\{g_L^2 + g_R^2\left(1 - \frac{T}{E_\nu}\right)^2 - \frac{g_L g_R m_e T}{E_\nu^2}\right\} \tag{1}$$

where m_e is the electron mass, $\sigma_0 = (2/\pi)(m_e \hbar c G_f)^2 = 8.77 \cdot 10^{-45}\mathrm{cm}^2, \mathrm{g_L} = \sin^2\theta_\mathrm{w} \pm 1/2$ (+ for ν_e, − for ν_μ or ν_τ), $\mathrm{g_R} = \sin^2\theta_\mathrm{w} \approx 0.23$ thus

$$\frac{d\sigma}{dT} = \left(\frac{\sigma_0}{m_e}\right)[i - sT + cT^2] \tag{2}$$

where the intercept $i = g_L^2 + g_R^2$, the slope $s = 2(g_R^2 + \varepsilon g_L g_R)/E_\nu$ and the quadratic slope $c = (g_R/E_\nu)^2$ with $\varepsilon = m_e/2E_\nu$. Hence, the intercept and linear slope depend on $g_{Le} = 0.73$ for ν_e interactions (NC + CC) or $g_{L\mu} = -0.27$ for ν_μ (or ν_τ) interaction (NC). Note that as $\varepsilon \to 0$, the slope becomes flavor independent ($s \to 2g_R^2/E_\nu$) but $i = g_L^2 + g_R^2$ remains flavor dependent. Assume, for a given E_ν, that the initial ν_e flux of neutrinos at the sun is ϕ. At the earth, the ν_e and non ν_e fluxes will be $\phi(1-f)$ and ϕf where $f = n_{\nu\mu}/(n_{\nu e} + n_{\nu\mu})$ is the mixing probability. The observable event distribution will then be

$$\begin{aligned}\frac{\Delta N}{\Delta T} &= K\phi\Big\{i_e(1-f)+i_\mu f+\Big[s_e(1-f)+s_\mu f\Big]T+cT^2\Big\}\\ &= K\phi\Big\{\Big[i_e-i_{e\mu}f\Big]+\Big[s_e-s_{e\mu}f\Big]T+cT^2\Big\}\end{aligned} \tag{3}$$

with $i_e = g_{Le}^2 + g_R^2, i_\mu = g_{L\mu}^2 + g_R^2, s_e = 2g_R(g_R + \varepsilon g_{Le})/E_\nu, s_\mu = 2g_R(g_R + \varepsilon g_{L\mu})/E_\nu$, $i_{e\mu} = i_e - i_\mu = 2g_R$ and $s_{e\mu} = s_e - s_\mu = 2\varepsilon g_R/E_\nu$.

Here $K = n_e(\sigma_0/m_e)\Delta t$ where n is the number of target electrons ($n_e \approx 2 \cdot 10^{30}$ in HELLAZ) and Δt is the data time interval. Integrating, we find n_i the counts expected in the ith bin in T (of width w) and n_{tot} total counts in m bins (of width mw) from j to k ($m = k - j + 1$).

$$n_i = K\phi w[a_i - b_i f] \tag{4}$$

$$n_{\text{tot}} = K\phi wm[d - ef] \tag{5}$$

where $a_i = i_e - s_e w(i - 1/2) + cw^2(i^2 - i + 1/3)$,
$b_i = i_{e\mu} - s_{e\mu} w(i - 1/2)$ and, letting $n = j - 1$:
$d = i_e - s_{e\mu} w(k + n)/2 + cw^2(k^2 + kn + n^2)/3$ and $e = i_{e\mu} - s_{e\mu} w(k + n)/2$.

We see from Eq. 5 that a measurement of n_{tot} suffices to determine f if the flux ϕ is known. This is the case for the pp (and p-e-p) solar neutrinos because ϕ_{pp} is practically fixed by the observed solar luminosity. However, we may generally eliminate the flux ϕ from Eq.'s (4, 5) to obtain an equation on the bin contents

$$n_i = \langle n\rangle \frac{a_i - b_i f}{d - ef} \tag{6}$$

Where $\langle n\rangle = n_{\text{tot}}/m$. This equation shows that $n_i/\langle n\rangle$ depends only on f since the coefficients (a_i, b_i, d, e) are known from electro-weak theory. This will be the basis of a least squares fit to the observed event distribution n_i. Note that f is determined from the observed data without reference to solar models of neutrino production. The absolute flux ϕ is then obtained from f and Eq.5. It can be directly compared to the solar models because it accounts for all the neutrinos and not just those seen by inverse β decay experiments. Note that for $E_\nu \gg m_e/2$ (i.e. for ^{7}Be neutrinos) the quantity $s_{e\mu} \to 0$ thus markedly lessening the sensitivity for independent determination of (f, ϕ).

Of course, if $f \neq 0$ is observed, this would show that neutrinos oscillate since only ν_e's are produced in solar nuclear reactions. Observation of non-zero f at several neutrino energies should suffice to separately determine the energy independent mixing probability

$\sin^2(2\theta)$ and the mass difference Δm^2 of the mixing neutrinos.

4.2 Sensitivity of the Flavor and Flux Determination

We have simulated the pp and ^{7}Be neutrino spectra in the HELLAZ detector ($n_e = 2 \cdot 10^{30}$) for a data taking time $\Delta t = 5$ years. We group the pp neutrinos into 4 bins of width $\Delta E_\nu = 50$ keV centered at $E_\nu = 245$, 295, 345, 395 keV with integrated fluxes $\phi = (1.10, 1.22, 1.14, 0.66).10^{10}\nu_e/\mathrm{cm}^2$-s, respectively [5]. These correspond to the expected sensitivity of HELLAZ to detect pp neutrinos i.e $220 < E_\nu < 420$ keV corresponding to $100 < T < 261$ keV. The expected events numbers for $T_{\min} = 50$ keV and no mixing ($f = 0$) are 1743, 3171, 4199 and 3099, respectively in the 4 bins of E_ν. For full mixing ($f = 1$) the corresponding event numbers are 547, 917, 1133 and 796, respectively. Already, if ϕ is known, we may discriminate, for example at $E_\nu = 295$ keV, between $f = 0$ with 3171 events and $f = 1$ with only 917 events. From Eq. 5 we solve for f to obtain

$$f = \frac{d}{e}\left(1 - \frac{n_{\mathrm{tot}}}{n_0}\right) \tag{7}$$

hence

$$\sigma_f = \left(\frac{d}{e}\right)\frac{\sqrt{n_{\mathrm{tot}}}}{n_0} \tag{8}$$

where $n_0 = K\phi mwd$ is the number of events for $f = 0$. Thus f will be known with an error between 1 and 3 % if the pp flux is assumed known. Without this assumption we can find f by minimizing the function

$$\chi^2 = \sum_i \left[\frac{n_i^{\mathrm{exp}} - n_i^{\mathrm{th}}}{\sigma_{n_i}}\right]^2 \tag{9}$$

where n_i^{th} is from Eq. 6. This procedure has been carried out with simulated data for HELLAZ with bin widths $w = (\sigma_{\mathrm{tx}} + \sigma_{\mathrm{tn}})/2$ where $\sigma_{\mathrm{tx}} = INT[(\sigma_T/T)T_{\max}] + 1$, $\sigma_{\mathrm{tn}} = INT([\sigma_T/T]T_{\min}) + 1$ and $\sigma_T/T = .03$. The results for the four 50 keV wide pp bins are shown in Figs. 6a-d.

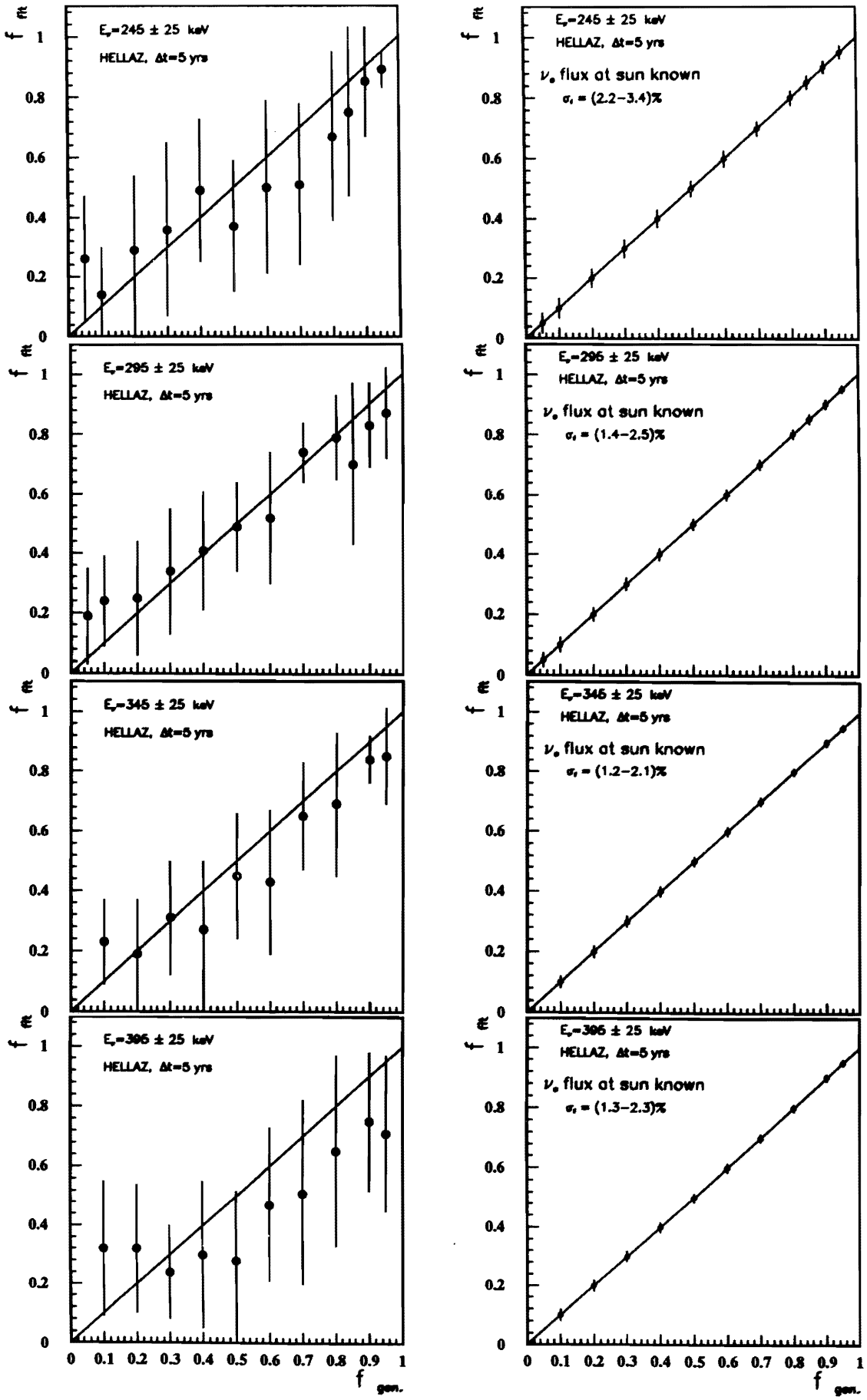

Figure 6: Left : fit f vs generated f. Right : fit f vs generated f assuming ϕ_{pp} is known.

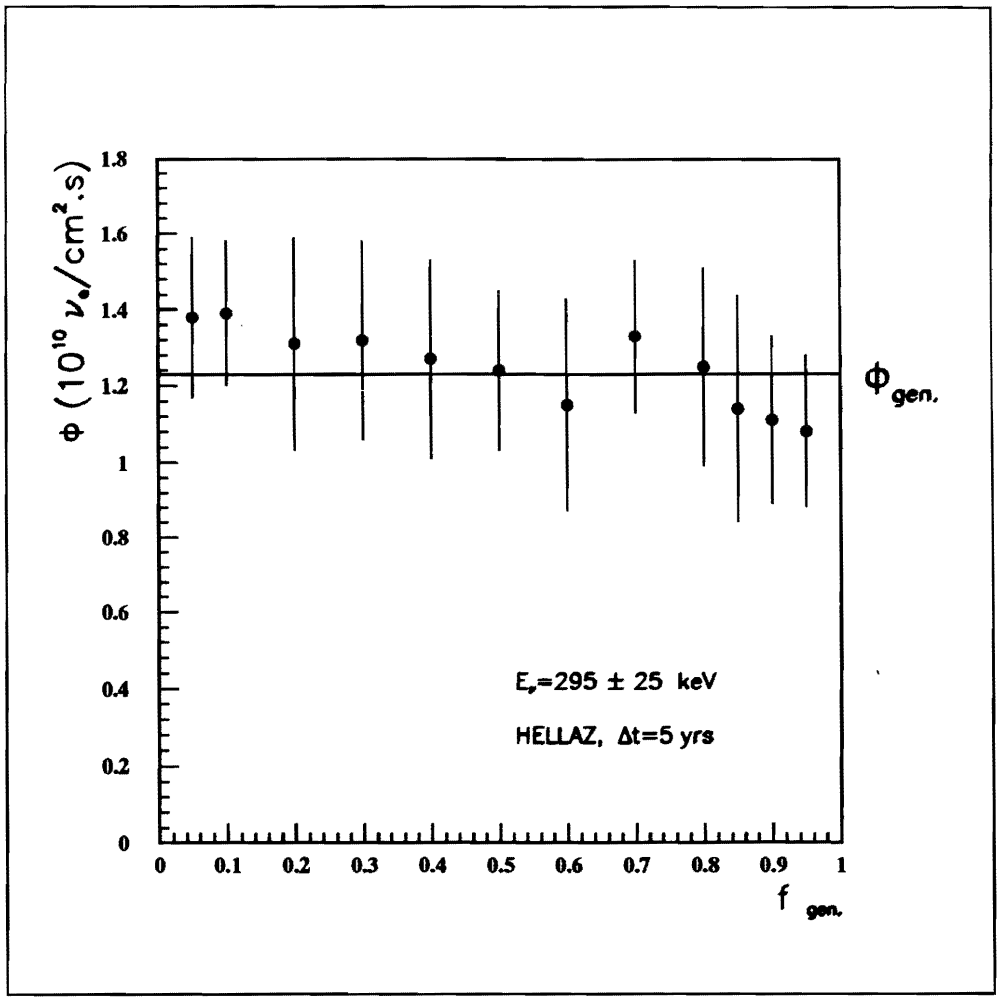

Figure 7: The flux ϕ vs generated f for $E_\nu = 295$ keV.

The left graph abcissa gives the assumed values of $f = f_{\rm gen}$ used to simulate the data and the ordinate gives the χ^2 minimization result $f = f_{\rm fit}$ with statistical errors (1σ). The right graph gives $f_{\rm fit}$ vs $f_{\rm gen}$ assuming the pp flux is known. Clearly, a 5 year HELLAZ run (left graph) will suffice to confirm the more accurate result (right graph) obtained assuming the pp flux known. Fig. 7 shows the flux $\phi = \phi_{\rm fit}$ as determined from $f = f_{\rm fit}$ and Eq. 5. This will verify the assumption of the pp flux to the indicated precision ($\approx 15\,\%$). Note, however, that f will be known to between 1 and 3 % if the pp flux is assumed known.

Assuming that a non-zero value of f has been obtained at several different neutrino energies, it will suffice to solve

$$f = \left(\frac{sin2\theta}{D_m}\right)^2 sin^2\left(\frac{\pi L D_m}{L_v}\right) \tag{10}$$

with

$$D_m = \sqrt{1 - 2\left(\frac{L_v}{L_m}\right)\cos 2\theta + \left(\frac{L_v}{L_m}\right)^2} \tag{11}$$

for the neutrino oscillation parameters $\sin^2(2\theta)$ and Δm^2. Here L is the neutrino flight distance (sun-earth or a fraction of the solar radius), $L_v = 4\hbar c E_\nu/\Delta m^2$ is the vacuum oscillation length and $L_m = 1/n_e r_0 \lambda_e$ is the matter oscillation length [5] (n_e is the sun's electron density, $r_0 = \sqrt{\pi\sigma_0} = 1.66 \cdot 10^{-22}$ cm and $\lambda_e = \hbar c/m_e = 3.86 \cdot 10^{-11}$ cm). Of course, a better strategy will be to fit all the pp spectral data simultaneously by inserting Eq. 10 into Eq. 9 and minimizing (the χ^2 or a likelihood function) directly with respect to $\sin^2(2\theta)$ and Δm^2. This type of extended analysis will not be attempted here.

We show in Fig. 8 the results of a HELLAZ simulation for $\Delta t = 20$ years or equivalently Mega HELLAZ (= Magna Graecia ?) for $\Delta t = 5$ years. This shows that long (or large) term verification is possible.

A similar simulation for the ^{7}Be neutrinos ($E_\nu = 862\,\text{keV}$ and $50 < T < 665\,\text{keV}$) is shown in Fig.9. It is seen that the sensitivity to determine f is so much reduced as to be useless (even for Mega HELLAZ). This is because the slope dependence of Eq. 2 vanishes as $\varepsilon = m_e/2E_\nu \to 0$ hence only n_{tot} is significant. We see from Eq. 5 that either a ϕ or f variation can give the same value of n_{tot} making it impossible to seperate these effects. Thus, since the ^{7}Be flux is uncertain, we conclude that understanding of the missing ^{7}Be neutrinos can only be obtained through the neutrino oscillation parameters as determined from the pp spectrum.

5 Conclusions and Perspective

We have reviewed the HELLAZ solar neutrino experiment proposal and have shown how the pp solar neutrino data can solve the solar neutrino problem. Several TPC prototypes have been constructed and are now under test. The collaboration is open and interested institutions are invited to make contact.

6 Acknowledgements

We wish to thank Prof. Marcel Froissart of Collège de France for his constant interest and support. Also thanks are due to Dr. Y. Giraud-Héraud of Collège de France for asking the question on the possibility of flavor discrimination.

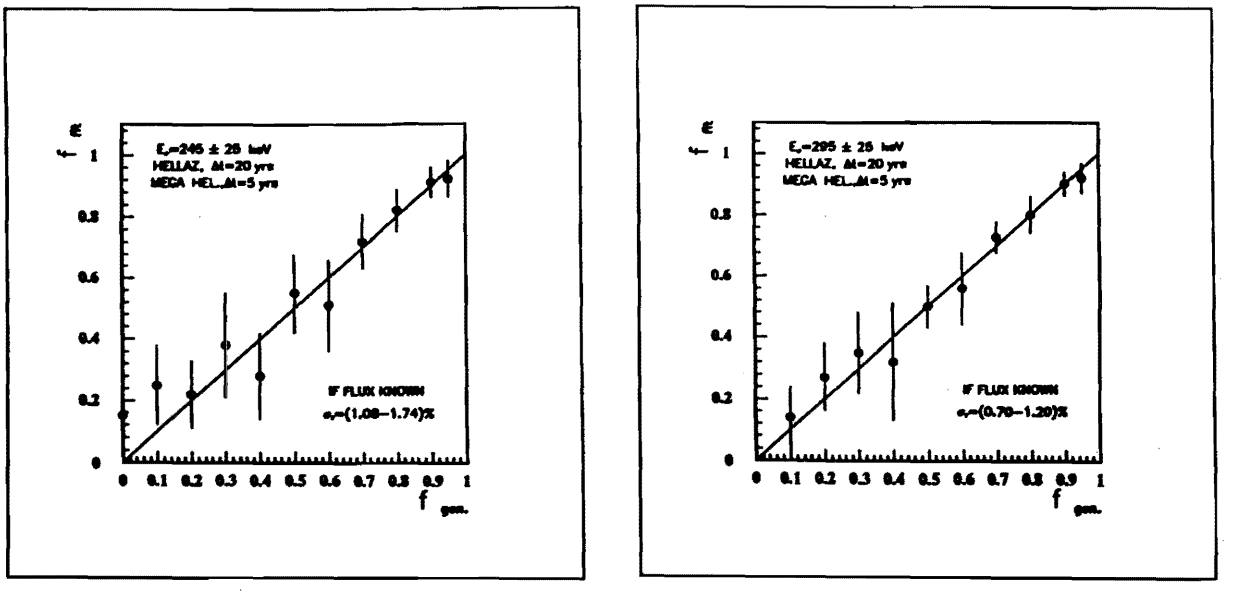

Figure 8: The fit f vs generated f for HELLAZ (20 y) or Mega HELLAZ (5 y).

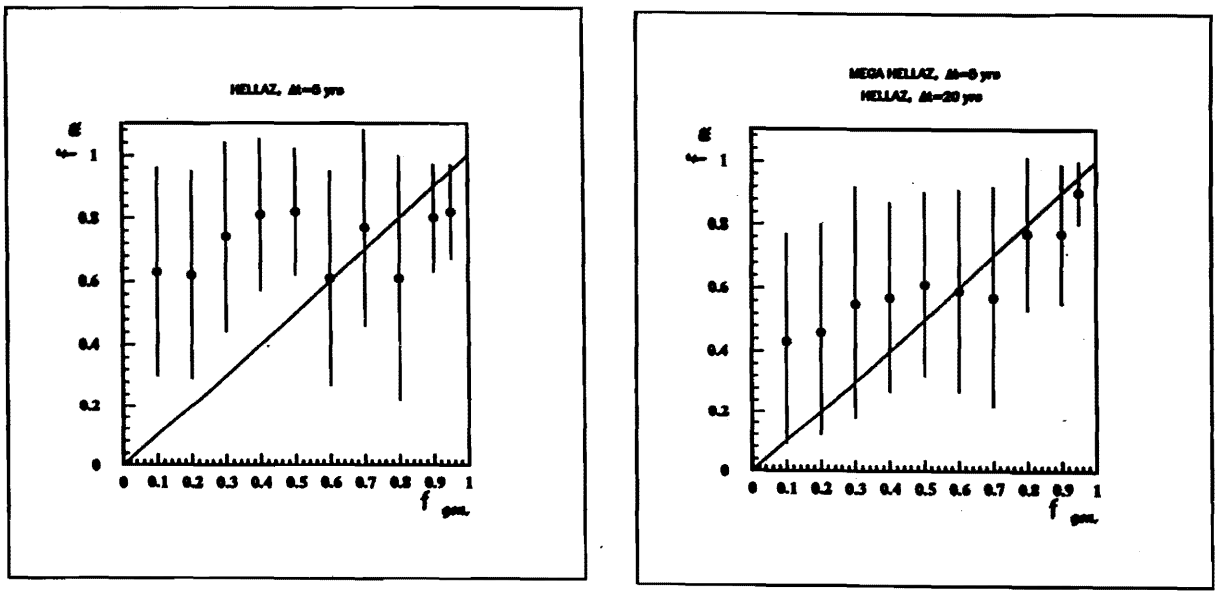

Figure 9: Fit f vs generated f for HELLAZ (5 y) or Mega HELLAZ (5y), $E_\nu = 862$ keV.

References

1. J. Séguinot, T. Ypsilantis and A. Zichichi, Collège de France, LPC/92-31, 12/8/92 and Proc. 4th Neutrino Telescope Workshop, Venezia, 10/3/92, pp. 289-313.

2. G. Laurenti et al., pp. 141-170, Proc. 2nd NESTOR Workshop, Pylos, 19-21/10/92. Here, the previous choice of a Liquid N_2 shield was replaced by a solid CO_2 to increase density and avoid buoyancy.

3. G. Laurenti et al., pp. 161-179 in Proc. 5th Neutrino Telescope Workshop, Venezia, 2-4/3/93 and

   G. Laurenti et al., pp. 213-242 in Proc. 17th Johns Hopkins Workshop on Current Problems in Particle Theory, "Particles and the Universe", Budapest 93, World Scientific.

   In these papers, a previous calculational error in the estimate of energy resolution was corrected from 20 % to 5 % for the pp neutrinos.

4. F. Arzarello et al., pp. 205-227, Proc. of the International School on Cosmological Dark Matter, Valencia, October 1993, World Scientific or Collège de France LPC/94-28 and CERN-LAA/94-19. Here the use of single electron sensitive TPC is proposed and investigated. This allows much denser sampling of the recoil track and potentially much better electron energy resolution.

5. J.H. Bahcall, Neutrino Astrophysics, Cambr. Univ. Press 1989.

6. HELLAZ Notes 92-01, 92-02, 92-03, G. Bonvicini, 3/11/92.

7. HELLAZ note 93-05, G. Bonvicini, 29/7/93.

8. R. Arnold et al., Nucl. Inst. and Meth. A314 (1992) 465.

9. D.V. Camin et al. Atlas Internal Note LARG-NO-11 (1994).

10. R. DeSalvo et al., Nucl. Instr. and Meth. A315 (1992) 375.

11. P. Weilhammer. Nucl. Instr. and Meth. A 342 (1994) 1.

12. O. Toker et al. Nucl. Instr. and Meth. A 340 (1994) 572.

13. GEANT Simulation Program, CERN-DD-E83-01.

14. A. Peisert and F. Sauli, CERN 84-08.

15. HELLAZ Note 7, F. Ciralli, 15/2/93.

16. G. t'Hooft, Phys. Rev. Letters, B37 (1971) 95.

17. J.H. Bahcall, Phys. Rev. Lett. 71 (1993) 2369 and IASSNS-AST 93-40, SCU 94-08.